

GEOMETRICALLY BASED CHANNEL MODEL FOR INDOOR RADIO PROPAGATION WITH DIRECTIONAL ANTENNAS

Y. Chen [†], Z. Zhang, and T. Qin

School of Computer, Electronics and Information
Guangxi University
Nanning 530004, China

Abstract—A geometrically based channel model is proposed to describe radio propagation in an indoor environment with directional antennas. In conventional geometric channel models (GCMs), distribution of scatterers does not take into account the antenna properties. A different approach is taken here for directional channel modeling. The locations of scattering objects are defined using non-Cartesian coordinates comprising an auxiliary geometric parameter ρ and angle-of-arrival (AOA) ϕ . Subsequently, we present a systematic method to study the influence of antenna pattern on scatterer distribution by applying two heuristic rules, which underpin the connection between the physical wave-propagation process and its canonical GCM. Provided with model preliminaries, important channel parameters including power azimuthal spectrum (PAS), power delay spectrum (PDS), mean effective gain (MEG), and antenna-decoupled PAS are derived and compared against the published data in the existing literature to demonstrate the usefulness of the proposed model.

1. INTRODUCTION

There has been a growing demand for indoor short-range communication systems such as millimeter-wave wireless personal area networks (WPANs) to provide high-speed multimedia data services in recent years [1–3]. It is commonly known that delay dispersion due to multipath propagation results in significant channel degradation. Furthermore, narrow beam antennas could be used to eliminate multipath,

Corresponding author: Y. Chen (Y.Chen@gre.ac.uk).

[†] Also with School of Engineering, University of Greenwich, Chatham Maritime, Kent, ME4 4TB, UK.

thereby allowing for the application of simple unequalized modulation schemes [4–7]. The advancement of smart antenna technology for space diversity has also motivated researchers to investigate the propagation phenomena in the space domain [8]. Hence, knowing the effects of antenna directivity on the channel characteristics is crucial for the evaluation of system performance.

Nonetheless, the influence of antenna radiation patterns has not been fully explored by researchers. For the case when angular distribution of energy around the radio access point (RAP) and user equipment (UE) is used (e.g., uniform [9], Gaussian [10] and more recently Laplacian [11–14]), the overall azimuthal response is obtained by multiplying the angle-resolved impulse response with the beam pattern [4]. On the other hand, if geometric channel models (GCMs) (e.g., [15–17]) are used to determine the channel properties, the antenna effect is usually accounted for by deleting those scatterers not within the antenna beam-scanning range [18–20].

In our previous work [21], it has been shown that the effect of directional antenna is twofold. Firstly, it alters the spatial distribution of scatterers by providing a different sample space for the random field and secondly, it collects the signal components from the angles-of-arrival (AOAs) by weighted combination. Hence, it will be more appropriate to present an antenna-dependent channel model by incorporating antenna properties in the model geometry, which will be the main objective of the current work. Different from [21] which emphasizes on macrocellular environments, focus here is placed on indoor short-range communications. The location of each scatterer \mathbf{S} is bijectively mapped to non-Cartesian coordinates (ρ, ϕ) . The variable ρ is an auxiliary geometric parameter, which is a function of the distance between the UE and \mathbf{S} , r_U , and the distance between \mathbf{S} and the RAP, r_R (see also Fig. 1). Furthermore, ϕ denotes the AOA at the RAP. This definition of scatterer position facilitates ready integration of antenna pattern into the model geometry as to be made clear in Section 2. As discussed in [22], typical WPAN involves predominantly azimuthal

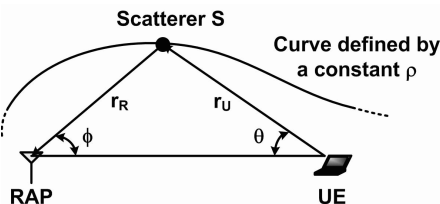


Figure 1. Non-Cartesian coordinates (ρ, ϕ) of scatterer location.

signal propagation. Therefore, the current work considers only two-dimensional propagation in line with other existing indoor channel models [22, 23].

The rest of the paper is organized as follows, Section 2 goes on to present two heuristic rules, which establish the relationship between the scatterer distribution $f_{\rho,\phi}(\rho, \phi)$ and the underlying physical environment [21, 24]. The versatile Von Mises angular distribution is proposed to model the antenna beam pattern because it includes or approximates many important functions like uniform, impulse, cardioid, and Gaussian [21]. The correspondence between scatterer and signal power distributions employs a variable exponent function to represent a wide variety of indoor propagation scenarios. Section 3 proceeds to derive important channel parameters including the power azimuthal spectrum (PAS), power delay spectrum (PDS), mean effective gain (MEG), and antenna-decoupled PAS. The validity of the proposed model is demonstrated through several numerical examples presented in Section 4. Finally, some concluding remarks are drawn in Section 5.

2. CHANNEL MODELING METHODOLOGIES

2.1. General Principles

Along the line of thought in [24], we define ρ in Fig. 1 as $\rho \triangleq r_R * r_U$. The operator $*$ represents either product or sum of the modulus of its arguments, depending on whether diffuse scattering or specular reflection dominates [24]. Apparently, the received power at the RAP from any scatterer \mathbf{S} is proportional to ρ^{-n} with n being the path loss exponent. Therefore, ρ is a measure of the mean path loss incurred by multipath components.

The following heuristic rules are postulated to underpin the connection between the geometric distribution of scatterers $f_{\rho,\phi}(\rho, \phi)$ and the power distribution in the channel $P(\rho, \phi)$. These rules are variation of the suppositions presented in [24] for narrowband nondirectional scenarios.

- *Rule 1:* Consider two scatterers located at (ρ_1, ϕ_1) and (ρ_2, ϕ_2) , respectively,

$$\frac{f_{\rho,\phi}(\rho_1, \phi_1)}{f_{\rho,\phi}(\rho_2, \phi_2)} = \frac{\xi(\rho_1, \phi_1)}{\xi(\rho_2, \phi_2)} \quad \text{if} \quad \frac{P(\rho_1, \phi_1)}{P(\rho_2, \phi_2)} = 1 \quad (1)$$

where $\xi(\rho_i, \phi_i)$ ($i = 1, 2$) is the *a priori* scatterer density at (ρ_i, ϕ_i) in the absence of transmit and receive antennas, and is assumed to be a constant $\frac{1}{\iint_{\Omega} d\rho d\phi}$ for all $(\rho, \phi) \in \Omega$ with Ω being the

integration domain of the scatterer distribution. $P(\rho_i, \phi_i)$ is the average power received at the RAP via scatterer (ρ_i, ϕ_i) .

- *Rule 2:* The mapping function implied in Rule 1, $f_{\rho, \phi}(\rho, \phi) = \mathcal{Z}(P(\rho, \phi))$ is a monotonically nondecreasing function.

Rule 1 asserts a one-to-one correspondence between the equi-scatterer-density curves and equi-power curves in the propagation channel. Rule 2 states that as the average received power at the RAP due to reradiation from a scatterer at a certain location decreases, the scatterer density at that location decreases as well. Given the antenna patterns at the RAP and UE, the principal relationship between the wave propagation process and the canonical model can be established by using the heuristic rules, thereby allowing for a systematic way of channel characterization.

2.2. Modeling of Antenna Patterns

The Von Mises probability density function (pdf) has been introduced to the communication community in various contexts. For example, it has been used to model the directional AOA of multipath components [25]. Let this function represent the directive gain of antennas at the RAP. After proper normalization, the Von Mises function becomes [21]

$$G(\phi) = \frac{\exp[\mu \cos(\phi - \phi_0)]}{I_0(\mu)} \quad (2)$$

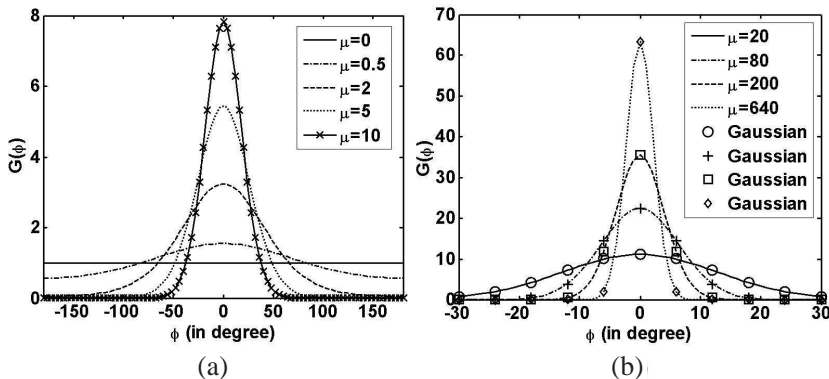


Figure 2. Von Mises pdfs for antenna patterns: (a) $\mu = 0, 0.5, 2, 5, 10$; and (b) $\mu = 20, 80, 200, 640$. The standard deviations of the Gaussian approximations in (b) are given by $1/\sqrt{\mu}$.

where $I_0(\mu)$ is the zero-order modified Bessel function, ϕ_0 represents the direction of maximum directive gain, and μ controls the width of the antenna beam. The pattern defined here is single-lobed over the whole angular region and any sidelobe structure is assumed to have a secondary effect. Fig. 2 depicts $G(\phi)$ in linear coordinates for different values of μ and $\phi_0 = 0$. As shown in Fig. 2, for $\mu = 0$, the antenna is isotropic; while $\mu \rightarrow \infty$ yields $G(\phi) \rightarrow \delta(\phi)$, where $\delta(\cdot)$ is the delta function representing an extremely narrow beam. For large μ , the inflexion points of $G(\phi)$ are approximately equal to $\pm 1/\sqrt{\mu}$. Therefore, for a unidirectional antenna beam pattern, the null-to-null beamwidth is roughly equal to $2/\sqrt{\mu}$. In addition, when μ is large the function resembles a Gaussian pdf with mean ϕ_0 and a standard deviation $1/\sqrt{\mu}$ as illustrated in Fig. 2(b).

2.3. Correspondence between $f_{\rho,\phi}(\rho, \phi)$ and $P(\rho, \phi)$

In indoor communication systems, antenna heights are relatively low. The RAP will receive multipath from scatterers distributed around the UE as well as itself. All angles in the azimuth plane are involved in this type of environment, and specular reflection is the major mechanism of the interaction between the electromagnetic waves and scatterers. Other mechanisms such as diffraction and diffuse scattering can be ignored [26]. In such cases, the operator $*$ refers to sum. Therefore, the curve representing a collection of scatterers with a constant ρ is an ellipse defined by $\{C : \rho = r_R + r_U = 2a\}$ as depicted in Fig. 3, where a is the semi-major axis of the ellipse. The RAP and UE are placed at the foci of the elliptical area with a distance of separation D .

Following Rule 1, there is a bijective mapping between the pdf $f_{\rho,\phi}(\rho, \phi)$ and $P(\rho, \phi)$. The function $f_{\rho,\phi}(\rho, \phi) = \mathcal{Z}(P(\rho, \phi))$ characterizes to what extent the scatterer distribution may be

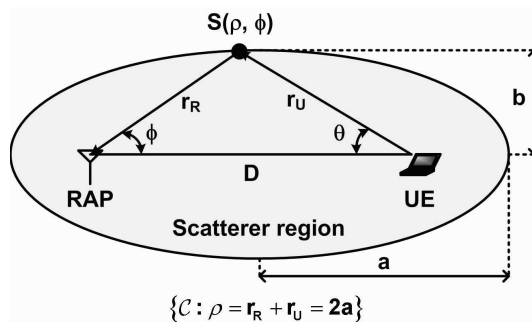


Figure 3. Elliptical scattering model.

influenced by the signal power. Furthermore, \mathcal{Z} has to be a monotonically nondecreasing function following Rule 2. Subsequently, we consider the following versatile function, which has been used to model the height profile of buildings inside the city layer [27]

$$\mathcal{Z}(P(\rho, \phi)) = \kappa(P_1, P_2, \gamma) \left\{ 1 - \left[\frac{P_2 - P(\rho, \phi)}{P_2 - P_1} \right]^\gamma \right\}, \quad P_1 \leq P \leq P_2 \quad (3)$$

where $\kappa(\cdot)$ is a normalization function to ensure that $\mathcal{Z}(\cdot)$ yields a pdf. $P(\rho, \phi) = \beta G(\phi) \rho^{-n}$ assuming that the directional antenna is only used at the RAP. However, the analysis can be easily extended to the situation when directional antennas are implemented at both ends of the radio link. $G(\cdot)$ denotes the antenna beam pattern as defined in (2), and β is the scattering coefficient modeled as a direction-insensitive parameter for simplicity. Subsequently, P_1 determines the minimum power below which the probability of finding an effective scatterer is zero, while P_2 is given by the maximum power contributed by all scatterers. Eq. (3) is plotted in Fig. 4. For $\gamma \ll 1$, $\mathcal{Z}(\cdot)$ describes the case when the occurrence of multipath components with power less than P_2 is rare, i.e., the arriving signals from most of the scatterers are at the level of maximum power, P_2 . The case when the distribution of scatterers becomes more uncorrelated with P is given by $\gamma \gg 1$. In the limiting case of $\gamma = 0$, all the scatterers have approximately the same power P_2 . For $\gamma \rightarrow \infty$, we have the case of multipath uniformly distributed between P_1 and P_2 .

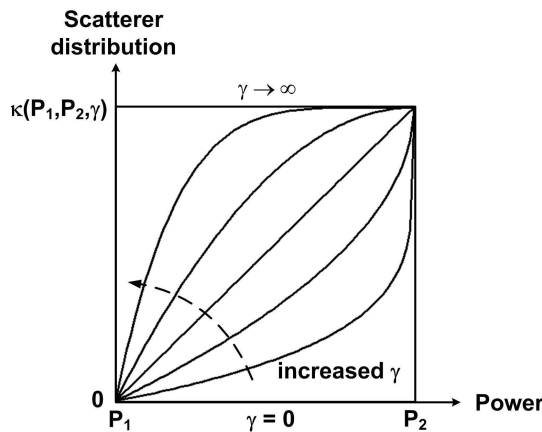


Figure 4. The function $\mathcal{Z}(\cdot)$ for various γ .

3. IMPORTANT CHANNEL PARAMETERS

3.1. PAS at the RAP and UE

Following the formulation in [14], the PAS at the RAP can be obtained as (see also Fig. 3)

$$\begin{aligned} \mathcal{P}_\phi(\phi) &= \Sigma_\phi \mathbb{E} \{P_s | \phi\} f_\phi(\phi) \\ &= \Sigma_\phi \left[\int_0^\infty \int_D P_s f_{P_s, \rho | \phi}(P_s, \rho | \phi) d\rho dP_s \right] f_\phi(\phi) \\ &= \Sigma_\phi \int_0^\infty \int_D P_s f_{P_s, \rho, \phi}(P_s, \rho, \phi) d\rho dP_s \end{aligned} \quad (4)$$

where Σ_ϕ is a normalization constant to ensure that $\mathcal{P}_\phi(\phi)$ is a pdf and P_s represents the instantaneous power received at the RAP. $\mathbb{E}(P_s | \phi)$ is the expected power of the waves conditioned on ϕ , $f_\phi(\phi)$ is the marginal pdf of ϕ , $f_{P_s, \rho | \phi}(P_s, \rho | \phi)$ is the joint pdf of P_s and ρ conditioned on ϕ , and $f_{P_s, \rho, \phi}(P_s, \rho, \phi)$ is the joint pdf of P_s , ρ , and ϕ . Let us assume that P_s is lognormally distributed [24] and is independent of the scatterer position. Consequently, the PAS in (4) can be derived as

$$\begin{aligned} \mathcal{P}_\phi(\phi) &= \Sigma_\phi \int_0^\infty \int_D P_s f_{P_s | \rho, \phi}(P_s | \rho, \phi) f_{\rho, \phi}(\rho, \phi) d\rho dP_s \\ &= \Sigma_\phi \int_D f_{\rho, \phi}(\rho, \phi) \left[\int_0^\infty P_s f_{P_s | \rho, \phi}(P_s | \rho, \phi) dP_s \right] d\rho \\ &= \Sigma_\phi \int_D f_{\rho, \phi}(\rho, \phi) \left[\beta G(\phi) \rho^{-n} \exp\left(\frac{\sigma_P^2}{2}\right) \right] d\rho \end{aligned} \quad (5)$$

where σ_P is the standard deviation of the lognormal fading around the RAP and UE, and is assumed to be direction-independent. $f_{P_s | \rho, \phi}(P_s | \rho, \phi)$ is the pdf of P_s conditioned on the scatterer location (ρ, ϕ) . Substituting (2) and (3) into (5) yields

$$\begin{aligned} \mathcal{P}_\phi(\phi) &= \Sigma'_\phi \int_D \left\{ 1 - \left[\frac{P_2 - \beta \exp(\mu \cos \phi) \rho^{-n} / I_0(\mu)}{P_2 - P_1} \right]^\gamma \right\} \\ &\quad \times \exp(\mu \cos \phi) \rho^{-n} d\rho \end{aligned} \quad (6)$$

with Σ'_ϕ being a normalization constant.

In order to determine the PAS at the UE, we need to acquire the joint pdf $f_{\rho, \theta}(\rho, \theta)$, where θ is the angle-of-departure (AOD) as shown in Fig. 3. This pdf can be evaluated using the following transformation

$$f_{\rho, \theta}(\rho, \theta) = \left. \frac{f_{\rho, \phi}(\rho, \phi)}{J(\phi)} \right|_{\phi=g(\rho, \theta)} \quad (7)$$

where $J(\phi)$ is the Jacobian transformation given by $J(\phi) = |d\phi/d\theta|^{-1}$. Based on the geometric relationship in Fig. 3, ϕ can be calculated as

$$\phi = g(\rho, \theta) = \cos^{-1} \left[\frac{2D\rho - (D^2 + \rho^2) \cos \theta}{D^2 - 2D\rho \cos \theta + \rho^2} \right] \quad (8)$$

Differentiating (8) gives the expression of $J(\phi)$. Following the same procedures used to derive the PAS at the RAP, the PAS at the UE is computed as

$$\begin{aligned} \mathcal{P}_\theta(\theta) &= \Sigma_\theta \mathbb{E} \{P_s | \theta\} f_\theta(\theta) \\ &= \Sigma_\theta \int_0^\infty \int_D P_s f_{P_s, \rho, \theta}(P_s, \rho, \theta) d\rho dP_s \\ &= \Sigma_\theta \int_D f_{\rho, \theta}(\rho, \theta) \left[\int_0^\infty P_s f_{P_s | \rho, \theta}(P_s | \rho, \theta) dP_s \right] d\rho \\ &= \Sigma_\theta \int_D \frac{f_{\rho, \phi}(\rho, \phi)}{J(\phi)} \left[\beta G(\phi) \rho^{-n} \exp\left(\frac{\sigma_P^2}{2}\right) \right] d\rho \Big|_{\phi=g(\rho, \theta)} \end{aligned} \quad (9)$$

where Σ_θ is a normalization factor to ensure that $\mathcal{P}_\theta(\theta)$ is a pdf. All the other terms in (9) are similarly defined following their counterparts in (4) and (5). Substituting (2), (3) and (8) into (9) yields

$$\begin{aligned} \mathcal{P}_\theta(\theta) &= \Sigma'_\theta \int_D \left\{ 1 - \left\{ \frac{P_2 - \beta \exp\{\mu \cos[g(\rho, \theta)]\} \rho^{-n} / I_0(\mu)}{P_2 - P_1} \right\}^\gamma \right\} \\ &\quad \times \exp\{\mu \cos[g(\rho, \theta)]\} \rho^{-n} \left| \frac{dg(\rho, \theta)}{d\theta} \right| d\rho \end{aligned} \quad (10)$$

with Σ'_θ being a normalization constant.

3.2. PDS

To evaluate the PDS, we first find the joint pdf $f_{\tau, \phi}(\tau, \phi)$ using

$$f_{\tau, \phi}(\tau, \phi) = c f_{\rho, \phi}(\rho, \phi) \Big|_{\rho=c\tau} \quad (11)$$

where τ is the path delay and c is the speed of electromagnetic waves. Following the same procedures used to derive the PAS, the PDS is

shown to be

$$\begin{aligned}
 \mathcal{P}_\tau(\tau) &= \Sigma_\tau \mathbb{E} \{ P_s | \tau \} f_\tau(\tau) \\
 &= \Sigma_\tau \int_0^\infty \int_{-\frac{1}{\sqrt{\mu}}}^{\frac{1}{\sqrt{\mu}}} P_s f_{P_s, \tau, \phi}(P_s, \tau, \phi) d\phi dP_s \\
 &= \Sigma_\tau \int_{-\frac{1}{\sqrt{\mu}}}^{\frac{1}{\sqrt{\mu}}} f_{\tau, \phi}(\tau, \phi) \left[\int_0^\infty P_s f_{P_s | \tau, \phi}(P_s | \tau, \phi) dP_s \right] d\phi \\
 &= \Sigma_\tau \int_{-\frac{1}{\sqrt{\mu}}}^{\frac{1}{\sqrt{\mu}}} f_{\tau, \phi}(\tau, \phi) \left[\beta G(\phi) (c\tau)^{-n} \exp\left(\frac{\sigma_P^2}{2}\right) \right] d\phi \\
 &= \Sigma'_\tau \int_{-\frac{1}{\sqrt{\mu}}}^{\frac{1}{\sqrt{\mu}}} \left\{ 1 - \left[\frac{P_2 - \beta \exp(\mu \cos \phi) (c\tau)^{-n} / I_0(\mu)}{P_2 - P_1} \right]^\gamma \right\} \\
 &\quad \times \exp(\mu \cos \phi) \tau^{-n} d\phi
 \end{aligned} \tag{12}$$

where Σ_τ and Σ'_τ are normalization factors. All the other terms in (12) are similarly defined following their counterparts in (4), (5) and (9). Finally, the delay spread is derived as the root second central moment of the PDS.

3.3. MEG of the RAP Antenna

It is well known that the MEG of antennas in a multipath environment cannot be accurately evaluated by using antenna directive gain only, since the non-isotropic angular response of the environment exists [28]. In order to infer channel behavior, we assume that the channel experiences quasi wide sense stationary uncorrelated scattering (QWSSUS) when the UE is moving along a random route in a local area. In other words, the UE moves only over a few wavelengths such that the directional characteristics of the environment response connecting the RAP and UE can be considered stationary. We further assume that the average over a random route in an environment is equivalent to the average over the environment (i.e., spatial ergodicity). Under this condition, the MEG of the RAP antenna can be defined following Taga's formulation [28]

$$G_e \triangleq \int_{-\pi}^{\pi} G(\phi) p_\phi(\phi) d\phi \tag{13}$$

In (13), $G(\phi)$ is the antenna beam pattern defined in (2) and $p_\phi(\phi)$ is the *antenna-decoupled* PAS, which is the angular response of the environment excluding the antenna effect, given by

$$p_\phi(\phi) = \frac{\alpha \mathcal{P}_\phi(\phi)}{G(\phi)} \tag{14}$$

where $\alpha = \left[\int_{-\pi}^{\pi} \mathcal{P}_{\phi}(\phi)/G(\phi)d\phi \right]^{-1}$ ensures that $p_{\phi}(\phi)$ is a pdf. Substituting (14) into (13) results in $G_e = \alpha$. It is worth noting that $p_{\phi}(\phi)$ is not defined independently from the antenna pattern in the current work.

4. NUMERICAL EXAMPLES

We present numerical examples for characteristics of indoor directional channels by applying the proposed model. The main purpose of this section is twofold. In Test Case 1 (TC1), the dependency of the antenna-decoupled PAS, MEG and PDS on the null-to-null beamwidth of the directive antenna at the RAP is studied. Four different values of μ are considered (cf. (2)). In Test Case 2 (TC2), we investigate the effect of different values of γ on the channel properties (cf. (3)). The parameters used in the numerical examples are listed in Table 1. The antenna parameter μ , the system operating frequency ω_0 , and the RAP-to-UE distance D are chosen to be comparable to the system conditions in the indoor empirical measurements in [6, 7]. The path loss exponent n is assumed to be 2, following the free space loss for each individual multipath component. However, it is more difficult to determine the values of γ and β due to the limited information provided in [6, 7] on the floor plan. As the main goal of the comparison with measurement in TC1 is to show whether the model developed could show the proper trends, the medium values of $\gamma = 1$ and $\beta = 0.5$ (i.e., 3dB average reflection loss) are used in TC1. In general, the scattering coefficient β can be estimated from the amount of obstacles present in the region as well as their reflection loss values. On the other hand, it would be useful to determine the values of γ in various indoor environments through more comprehensive measurement campaigns, which would benefit from the theoretical analysis presented in the current work.

Table 1. Parameters used in the test cases.

Symbols	Numerical Values (TC1)	Numerical Values (TC2)
μ	[0 2 80 200]	10
ω_0	60 GHz	60 GHz
\mathbf{n}	2	2
γ	1	[0.1 1 10]
\mathbf{D}	10 m	10 m
β	0.5	0.5

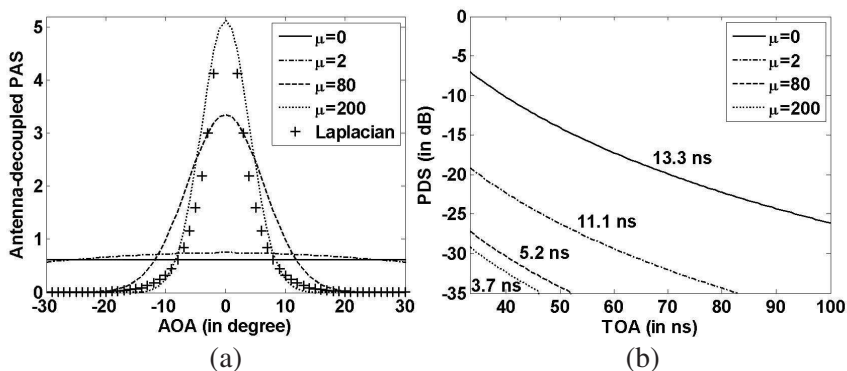


Figure 5. (a) Antenna-decoupled PAS and (b) PDS at the RAP in TC1. The corresponding delay spreads for various PDS are also shown in (b).

The antenna-decoupled PAS at the RAP, $p_\phi(\phi)$, in TC1 is shown in Fig. 5(a). As can be seen from Fig. 5(a), $p_\phi(\phi)$ peaks at $\phi = 0^\circ$ [line-of-sight (LOS) path] and decreases as the AOA deviates from the LOS path. It is also found that the profile of $p_\phi(\phi)$ changes as the antenna becomes more directive, which reaffirms the statement made earlier in Section 1. The effect of using directional sensors is twofold. Firstly, it reshuffles the spatial distribution of scatterers and secondly, it collects signal power by weighted combination. Furthermore, when μ is large, $p_\phi(\phi)$ shows a good agreement with a Laplacian distribution with an azimuth spread of 14° . This phenomenon has already been observed in various indoor measurements [12, 13]. As μ decreases, $p_\phi(\phi)$ starts to deviate from a standard Laplacian pdf. The corresponding MEGs are calculated to be $G_e = 1.0, 2.8, 16.2, 26.0$ for $\mu = 0, 2, 80, 200$, indicating that the MEG increases with μ .

Figure 5(b) shows the PDS for different antenna beamwidths. It is found that the delay dispersion is significantly reduced when the receive antenna becomes more directive, which is comparable to the observations made in [5–7]. In order to establish the validity of the proposed model, we further compare the theoretical delay spreads to the experimental and simulated data in [6]. Manabe et al. conducted indoor propagation measurements at 60 GHz in a modern office room and compared the experimental results with three-dimensional ray-tracing simulations, which took into account the effects of polarization and antenna directivity [6]. The floor area is $13.51 \text{ m} \times 7.81 \text{ m}$, and the ceiling is about 2.6 m above the floor. During measurements,

the room was kept empty, with no furniture except a transmitter, receiver, and some other experimental equipment. A transmitter with an omnidirectional antenna was located 24 cm below the ceiling at the center of the room, and the measurements were carried out at several receiving positions within the room. The receiving end was implemented using four types of antennas: an omnidirectional antenna and three directive antennas with wide (scalar feed horn), medium (pyramidal standard horn), and narrow (scalar lens horn) beams, respectively. The comparisons are summarized in Table 2 and it can be concluded that the model results are in good agreement with the empirical and simulated data.

Figure 6 shows the antenna-decoupled PAS and PDS for TC2. The angular and delay spreads increase with γ . This phenomenon implies that when the power of multipath components is more uniformly distributed between P_1 and P_2 , the power of ray arrivals is more widely spread in the azimuth and delay domains. The results also demonstrate a positive correlation between the angular and delay spreads. The same observations have been made in the outdoor measurement [29]. Furthermore, the results also indicate that the mechanisms leading to azimuthal and temporal dispersions are related. Therefore, the spatial and frequency diversity gains for short-range indoor communication systems are highly interrelated. The corresponding MEGs are found to be $G_e = 5.9, 5.6, 4.7$ for $\gamma = 0.1, 1, 10$, indicating that the MEG decreases as γ increases.

Table 2. Comparison of the measured [6], simulated [6], and theoretical delay spreads for different types of antennas.

Antenna Type	Beamwidth	Main Beam	Delay Spread		
			Measured	Simulated	Theoretical
Omni ($\mu = 0$)		$\lambda/2$ dipole (Von Mises)	18.1 ns	15.4 ns	13.3 ns
Wide ($\mu = 2$)	60° (81°)	Gaussian (Von Mises)	13.6 ns	10.9 ns	11.1 ns
Medium ($\mu = 80$)	10° (13°)	Pyramidal horn (Von Mises)	4.7 ns	2.2 ns	5.2 ns
Narrow ($\mu = 200$)	5° (8°)	Gaussian (Von Mises)	1.1 ns	0.8 ns	3.7 ns

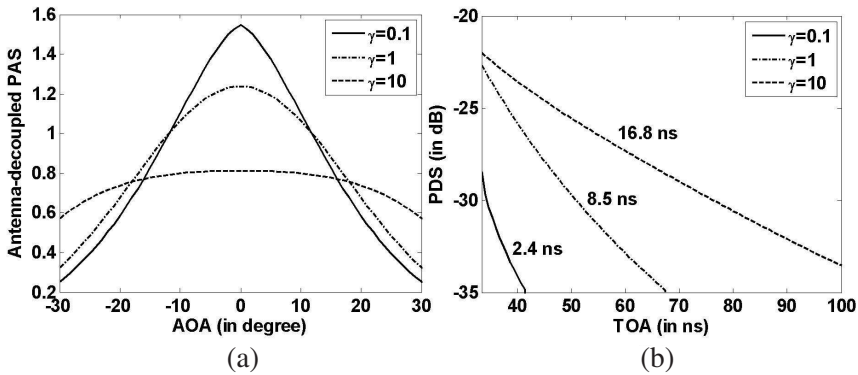


Figure 6. (a) Antenna-decoupled PAS and (b) PDS at the RAP in TC2. The corresponding delay spreads for various PDS are also shown in (b).

5. CONCLUSIONS

A novel GCM for indoor radio propagation with directional antennas has been presented. The Von Mises function that includes a wide variety of nonisotropic scenarios was proposed to describe the beam shapes and the variable exponent function was used to model the relationship between the scatterer distribution and power distribution. Important channel properties including PAS, PDS, MEG, and antenna-decoupled PAS were then derived. We have also compared the theoretical delay spreads to the published data. A good agreement between the theoretical and measured/simulated results has been observed, which demonstrates the effectiveness of the proposed model. The analytical framework presented in this paper would be useful for first-stage system design and performance evaluation when directional antennas are to be implemented in an indoor communication system.

REFERENCES

1. Khaddaj Mallat, N., E. Moldovan, and S. O. Tatu, "Comparative demodulation results for six-port and conventional 60 GHz direct conversion receivers," *Progress In Electromagnetics Research*, PIER 84, 437–449, 2008.
2. Costanzo, S., I. Venneri, G. Di Massa, and G. Amendola, "Hybrid array antenna for broadband millimeter-wave applications," *Progress In Electromagnetics Research*, PIER 83, 173–183, 2008.

3. Wells, J., "Faster than fiber: The future of multi-Gb/s wireless," *IEEE Microwave Magazine*, Vol. 10, 104–112, May 2009.
4. Yang, H., M. H. A. J. Herben, I. J. A. G. Akkermans, and P. F. M. Smulders, "Impact analysis of directional antennas and multiantenna beamformers on radio transmission," *IEEE Trans. Veh. Technol.*, Vol. 57, 1695–1797, May 2008.
5. Dabin, J. A., A. M. Haimovich, and H. Grebel, "A statistical ultra-wideband indoor channel model and the effects of antenna directivity on path loss and multipath propagation," *IEEE J. Sel. Areas Commun.*, Vol. 24, 752–758, Apr. 2006.
6. Manabe, T., Y. Miura, and T. Ihara, "Effects of antenna directivity and polarization on indoor multipath propagation characteristics at 60 GHz," *IEEE J. Sel. Areas Commun.*, Vol. 14, 441–448, Apr. 1996.
7. Rappaport, T. S. and D. A. Hawbaker, "Wide-band microwave propagation parameters using circular and linear polarized antennas for indoor wireless channels," *IEEE Trans. Commun.*, Vol. 40, 240–245, Feb. 1992.
8. Molisch, A. F., H. Asplund, R. Heddergott, M. Steinbauer, and T. Zwick, "The COST259 directional channel model — Part I: Overview and methodology," *IEEE Trans. Wireless Commun.*, Vol. 5, 3421–3433, Dec. 2006.
9. Clarke, R. H., "Multiple diversity theory of mobile radio reception," *Bell Syst. Tech. J.*, 967–1000, Jul./Aug. 1968.
10. Vaughan, R., "Spaced directive antennas for mobile communications by the Fourier Transform Method," *IEEE Trans. Antennas Propagat.*, Vol. 48, 1025–1032, Jul. 2000.
11. Zhang, Y., A. K. Brown, W. Q. Malik, and D. J. Edwards, "High resolution 3-D angle of arrival determination for indoor UWB multipath propagation," *IEEE Trans. Wireless Commun.*, Vol. 7, 3047–3055, Aug. 2008.
12. Poon, A. and M. Ho, "Indoor multiple-antenna channel characterization from 2 to 8 GHz," *Proc. IEEE ICC, Anchorage, AK*, 3519–3523, May 2003.
13. Cramer, R. J.-M., R. A. Scholtz, and M. Z. Win, "An evaluation of the ultra-wide band propagation channel," *IEEE Trans. Antennas Propagat.*, Vol. 50, 561–570, May 2002.
14. Pedersen, K., P. Mogensen, and B. Fleury, "A stochastic model of the temporal and azimuthal dispersion seen at the base station in outdoor propagation environments," *IEEE Trans. Veh. Technol.*, Vol. 49, 437–447, Mar. 2000.

15. Liberti, J. C. and T. S. Rappaport, "A geometrically based model for line of sight multipath radio channels," *Proc. IEEE Veh. Technol. Conf.*, 844–848, Apr. 1996.
16. Jiang, L. and S. Y. Tan, "Geometrically based statistical channel models for outdoor and indoor propagation environments," *IEEE Trans. Veh. Technol.*, Vol. 56, 3587–3593, Nov. 2007.
17. Khan, N. M., M. T. Simsim, and P. B. Rapajic, "A generalized model for the spatial characteristics of the cellular mobile channel," *IEEE Trans. Veh. Technol.*, Vol. 57, 22–37, Jan. 2008.
18. Petrus, P., J. H. Reed, and T. S. Rappaport, "Geometrical-based statistical macrocell channel model for mobile environments," *IEEE Trans. Commun.*, Vol. 50, 495–502, Mar. 2002.
19. Fuhl, J., A. Molisch, and E. Bonek, "Unified channel model for mobile radio systems with smart antennas," *IEE Proc. - Radar, Sonar Navig.*, Vol. 145, 32–41, Feb. 1998.
20. Amoroso, F. and W. W. Jones, "Geometric model for DSPN satellite reception in the dense scatterer mobile environment," *IEEE Trans. Commun.*, Vol. 41, 450–453, Mar. 1993.
21. Chen, Y., Z. Zhang, and V. K. Dubey, "Effect of antenna directivity on angular power distribution at mobile terminal in urban macrocells: A geometric channel modeling approach," *Wireless Personal Communications*, Vol. 43, 389–409, 2007.
22. Chen, Y., Z. Zhang, L. Hu, and P. Rapajic, "Geometry-based statistical model for radio propagation in rectangular office buildings," *Progress In Electromagnetics Research B*, Vol. 17, 187–212, 2009.
23. Janaswamy, R., "An indoor pathloss model at 60 GHz based on transport theory," *IEEE Antennas Wirel. Propagat. Lett.*, Vol. 5, 58–60, 2006.
24. Chen, Y. and V. K. Dubey, "Accuracy of geometric channel-modeling methods," *IEEE Trans. Veh. Technol.*, Vol. 53, 82–93, Jan. 2004.
25. Abdi, A., J. A. Barger, and M. Kaveh, "A parametric model for the distribution of the angle of arrival and the associated correlation function and power spectrum at the mobile station," *IEEE Trans. Veh. Technol.*, Vol. 51, 425–434, May 2002.
26. Ertel, R. B., P. Cardieri, K. W. Sowerby, T. S. Rappaport, and J. H. Reed, "Overview of spatial channel models for antenna array communication systems," *IEEE Personal Communications*, Vol. 5, 10–22, Feb. 1998.
27. Blaunstein, N., D. Katz, D. Censor, A. Freedman, I. Matityahu,

- and I. Gur-Arie, "Prediction of loss characteristics in built-up areas with various buildings overlay profiles," *IEEE Antennas and Propagation Magazine*, Vol. 43, 181–191, Dec. 2001.
28. Taga, T., "Analysis for mean effective gain of mobile antennas in land mobile radio environments," *IEEE Trans. Veh. Technol.*, Vol. 39, 117–131, May 1990.
 29. Algans, A., K. I. Pedersen, and P. E. Mogensen, "Experimental analysis of the joint statistical properties of azimuth spread, delay spread, and shadow fading," *IEEE J. Select. Areas Commun.*, Vol. 20, 523–531, Apr. 2002.